# The effect of active vibration control on the sound field scattered from a flexible structure

**C. House, J. Cheer, S. Daley**
Institute of Sound and Vibration Research - University of Southampton
e-mail: **c.house@soton.ac.uk**

## Abstract

It is desirable, in many applications, to minimise the acoustic scattering from an object when it is subject to an incident sound field. Active Vibration Control (AVC) has been demonstrated in many applications, and can effectively reduce an unwanted disturbance signal using control sources. However, when attempting to attenuate the acoustic scattering from an object, it is not straightforward to measure, and therefore control, the scattered component of the sound field directly. In this paper, the effect that AVC has on the scattered acoustic field has been investigated for a hollow, non-rigid cylinder via a series of numerical simulations. The cylinder is excited by an acoustic plane wave incident from a single direction and the AVC system uses an array of accelerometers and an array of structural actuators to control the vibration. As expected, significant reductions in the structural velocity are predicted. The effect of AVC on the acoustic scattering is then investigated, and it is shown that, at resonance, the scattered sound power is reduced by over 5dB.

## 1 Introduction

Active control has now been demonstrated and applied to many applications, and has been shown to be effective at reducing a range of different disturbance signals with the introduction of secondary control sources. In the case of active acoustic cloaking, the disturbance signal to be minimised is the scattered sound pressure, as shown in Figure 1, which could be controlled using either structural or acoustic control sources. This has been demonstrated numerically by Eggler [1] and Cheer [2], who present results using computational models that predict significant reductions in the acoustic scattered field over a fairly wide frequency range by using secondary acoustic sources [2], and secondary structural sources [1]. However, the performance of an active control system is dependent on the measured disturbance signal, and in the case of acoustic cloaking it is not possible to measure the scattered component of the sound field directly in real-time. Therefore it is challenging to minimise acoustic scattering directly,

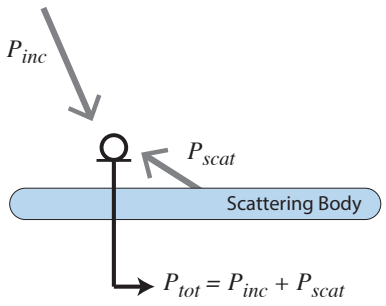


Figure 1: A schematic diagram of a microphone measuring a sound field including scattering.

Friot et al [3] have predicted and demonstrated a potential solution to this scattered field detection problem, with the development of an active control system that was two concentric rings of microphones surrounding the scattering object. The correlation between each ring was used to determine the incident signal from the scattered signal. This performs very well in the computer simulation at low frequencies, with reductions in the scattered field of an order of magnitude; however it is less effective at higher frequencies. The model was validated with a simple 1D experiment in a duct, and over 20dB of attenuation was achieved in the scattered pressure between 100Hz and 700Hz. Friot et al went on to implement a three dimensional single-tone control system based on this theory [4] with a parallelepiped scattering object, and achieved reductions in the scattered field of between 5dB and 20dB.

Although Friot et al were able to demonstrate a cloaking capability, the system required a large number of microphones positioned remotely from the structure to accurately distinguish the incident and scattered pressure waves, which may not always be practical to implement. Han et al [5] eliminate the need for the second ring of error sensors by modelling the transfer function between the scattered pressure and the total pressure with a computational model. They then use the simulated transfer function to estimate the scattered component of the microphone signals, which is then used as the disturbance signals for the active control system. The structure was implemented in a laboratory experiment using a spherical scatterer, and an 8dB attenuation in the scattered pressure was demonstrated.

It should be noted that Han's experiments were using simplified 1D active control systems, and only corrected for reflective scattering (reducing scattering in the opposite direction to the propagation of the incident wave). They did not attempt to reduce refractive scattering (scattering 'downstream' of the scattering object). They were also only excited by a single tone, single direction incident wave. In practice, there is an interest in controlling the scattering due to uncorrelated disturbance sources at multiple positions over a broad bandwidth and this would significantly deteriorate performance.

To attempt to overcome some of the practical limitations of directly controlling scattering, the effect of active vibration control on the acoustic scattering from a controlled body is investigated in this paper. The benefit of this method is that real-time adaptive active vibration control has been more extensively investigated and demonstrated, and has now matured into a robust and regularly used real-world solution to vibration problems [6, 7, 8, 9]. Initially, the development of a numerical model to predict the vibro-acoustic properties of a flexible cylinder will be discussed. A modal analysis will be carried out to identify the eigenfrequencies and mode shapes of the cylinder, before the structural response of the cylinder to an incident acoustic plane wave is modelled. The acoustic scattered field is calculated, and a formulation for the total acoustic scattered power is used at each frequency to compare the magnitude of the acoustic scattering to the magnitude of the structural response. Single tone active vibration control is simulated, and the effect that this has on the scattered acoustic field is predicted.

## 2 Numerical Model of Structural-Acoustic Coupled System

The COMSOL Multiphysics package has been used to model the structural-acoustic response of of a flexible hollow cylinder. The Boundary Element Method (BEM) was used to model the incident plane wave, whilst the Finite Element Method (FEM) was used to model structural vibration through the cylindrical shell, and acoustic propagation within the internal cavity of the cylinder. The use of BEM to model the incident and scattered acoustic waves in the external fluid significantly reduced the computational cost of solving the model when compared to FEM. This advantage is minimal for small problem sizes, however, therefore the interior volume of the cylinder was modelled using FEM so as to mesh well with the solid shell and therefore minimise the amount of BEM/FEM coupling required.

## 2.1 Model Description

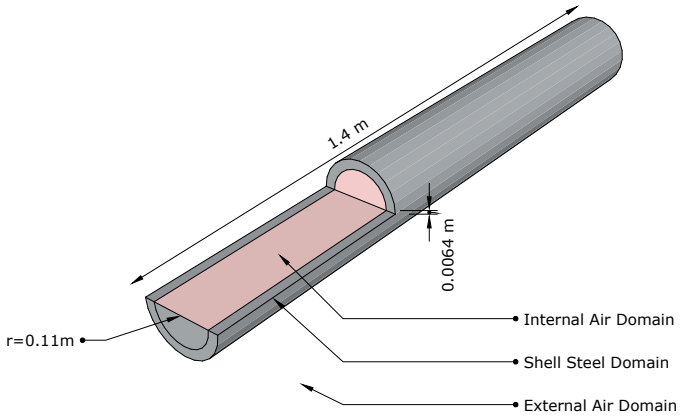


Figure 2: Cylinder Geometry

A steel cylindrical shell of thickness 6.4mm, length 1.4m and radius 0.11m has been modelled, and the geometry is shown in Figure 2. The internal volume of the cylinder was filled with air, and the the external fluid in which the cylinder was placed was also air. Acoustic propagation through both the internal and external air domains was modelled, as was structural vibration through the steel domain, with both physics being fully coupled to allow for the transfer of energy between acoustic and structural excitations. The structure was excited by a single incident acoustic plane wave, propagating from the $\theta = 45$ $\phi = 45$ direction, as shown in Figure 3.

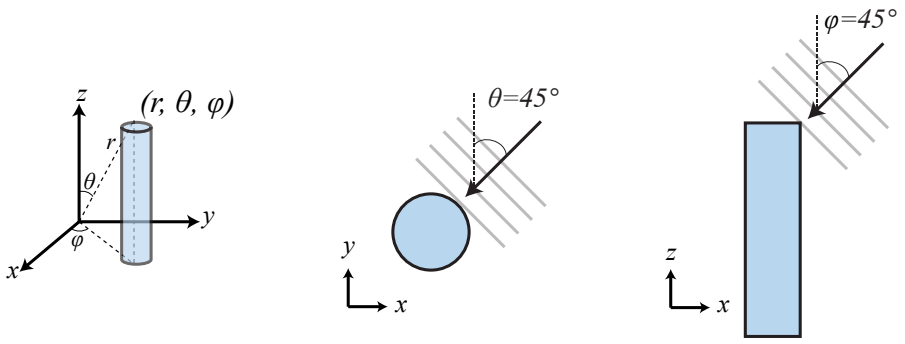


Figure 3: Schematic diagram showing the direction of the incident acoustic plane wave, in both plan view and front projection.

The model was meshed using free tetrahedral elements over the cylindrical shell, with a minimum of 6 elements per wavelength. This mesh density was selected as a result of a convergence study, which showed that 6 elements per wavelength was sufficient to obtain reliable results. The external air domain does not require meshing due to the use of BEM rather than FEM.

## 2.2 Modal Analysis

It is well known that the structural response of the cylinder will be greatest when it is excited at a resonance, and the work by Bobrovnitskii [10] and Williams [11] shows that the acoustic scattering of a structure

may also increase around these resonant frequencies. To identify the frequencies at which this will occur, an eigenfrequency analysis was conducted using the implemented numerical model. The modal frequencies, and corresponding mode shapes, were calculated and used to inform further analysis on the structural response of the cylindrical shell. The identified eigenfrequencies below 1kHz are shown in Table 1; axisymmetric, repeated modes have only been included once but are indicated by bold typeface.

An analytical model of a rigid walled cylindrical acoustic cavity was also solved [12] to indicate the eigenfrequencies of such a system. These results were used to distinguish whether the frequencies identified in the numerical model were caused by acoustic cavity modes, or structural modes. This has also been noted in Table 1.

Figure 4 displays the mode shapes of a selection of the modes identified in Table 1, which result in the largest structural response. As before, axisymmetric, repeated modes have only been included once but are identified by bold typeface.

| **Eigenfrequency** (Hz) | **Cause** |
|---|---|
| 122 | Cavity Mode |
| 245 | Cavity Mode |
| **353** | **Structural Mode** |
| 367 | Cavity Mode |
| 490 | Cavity Mode |
| **512** | **Structural Mode** |
| **548** | **Structural Mode** |
| 612 | Cavity Mode |
| 735 | Cavity Mode |
| 858 | Cavity Mode |
| **860** | **Structural Mode** |
| **915** | **Cavity Mode** |
| **923** | **Cavity Mode** |
| **947** | **Cavity Mode** |
| **948** | **Structural Mode** |
| **980** | **Cavity Mode** |
| 981 | Structural Mode |
| **985** | **Cavity Mode** |

Table 1: Modal frequencies below 1kHz, and whether they are caused by acoustic or structural resonances. Bold font represents an axisymmetric repeated mode.

The output from this modal analysis provides an indication of at which frequencies the structural velocity will be at a maxima, and therefore, at which frequencies acoustic scattering will potentially be most significant. These frequencies will be the most important to acoustic cloaking applications. The mode shapes shown in Figure 4 also assist in the future implementation of AVC, as they provide physical insight into which positions on the cylinder will be the most efficient for placement of accelerometers and actuators for the control of a particular mode.

## 2.3 Structural Response to an Acoustic Excitation

The vibro-acoustic model has been solved over a fine frequency sweep from 100Hz to 1kHz. At each frequency point the squared radial velocity when excited by a single incident plant wave has been integrated

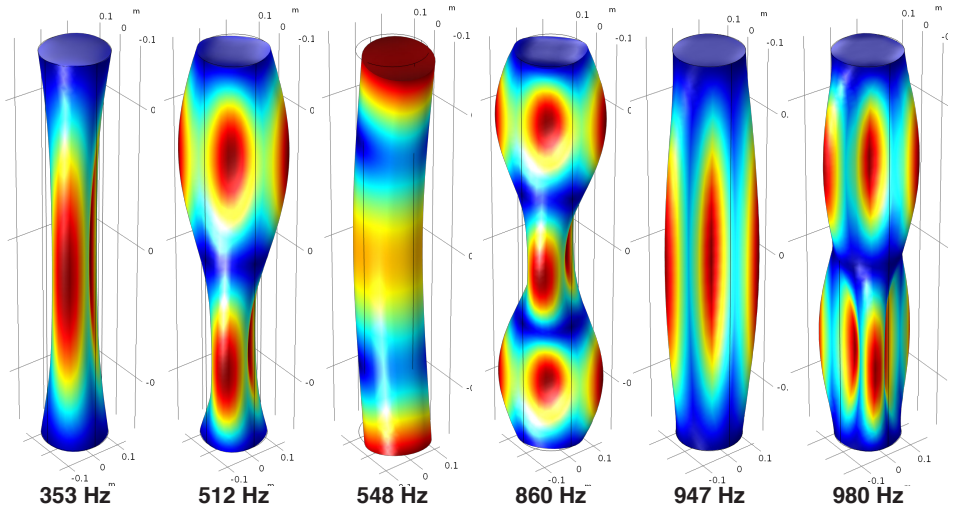


Figure 4: A selection of the modal frequencies and corresponding mode shapes of the cylinder. Frequencies in bold indicate that mode is a repeated axisymmetric mode.

over the cylindrical shell to calculate the resultant Kinetic Energy. This is shown in Figure 5, along with dashed vertical lines marking the eigenfrequencies calculated previously. It can be seen that there are 6 dominant resonances in the structure which, when compared to the mode shapes shown in Figure 4, all correspond to structural bending or acoustic breathing modes of the cylinder. The largest resonance is at 548Hz, and corresponds to the first acoustic bending mode of the cylinder.

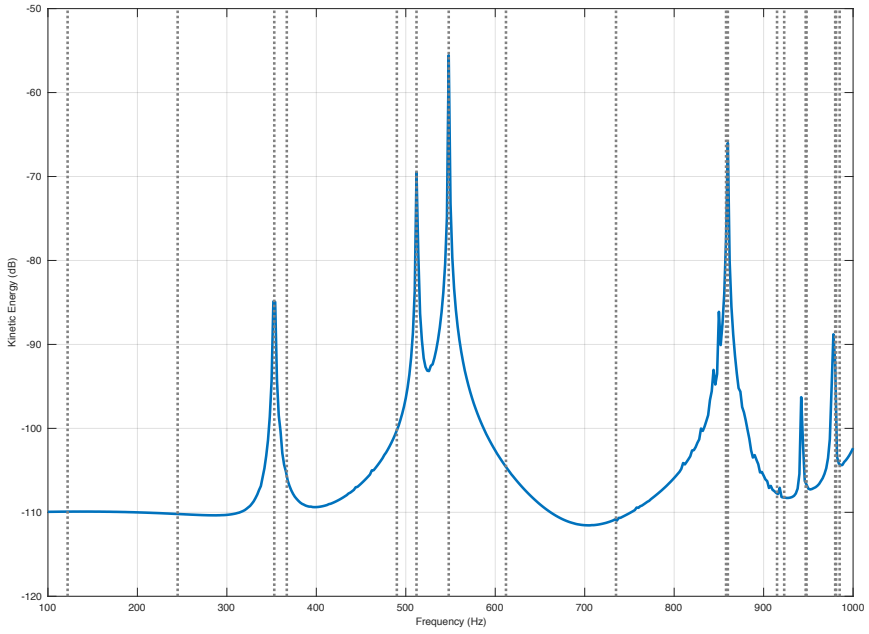


Figure 5: Kinetic energy of the cylinder as a function of frequency, when excited by an acoustic plane wave from $\theta = 45$ $\phi = 45$. Dashed vertical lines identify the frequencies of the modes of the cylinder.

## 2.4 Scattered Acoustic Response

The results presented above describe the structural response to an acoustic excitation. Now, the effect that this has on the acoustic pressure field will be investigated. To begin with, the computational model was solved at the four highest magnitude resonance frequencies identified in Figure 5. In each case the total acoustic pressure field $p_t$ has been plotted over a $1\mathrm{m} \times 1\mathrm{m}$ grid with the cylinder marked in black and the angle of incidence marked with an arrow, as shown in Figure 6. These plots show that the presence of the cylinder is generating two types of acoustic scattering: acoustic reflections and acoustic shadowing, especially at the 548Hz mode.

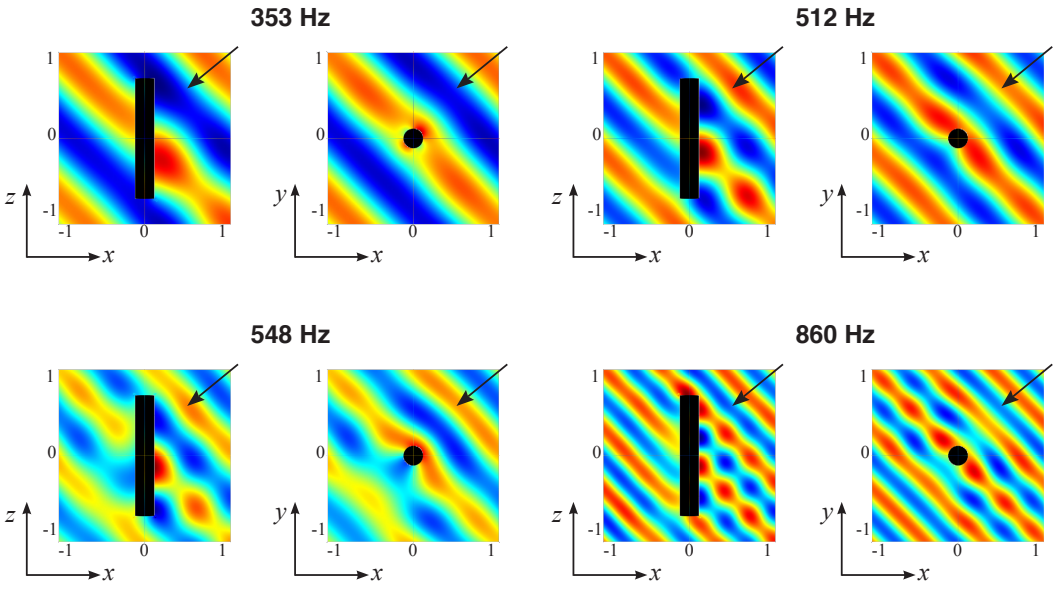


Figure 6: Predicted acoustic pressure field when the cylinder is excited by an incident plane wave at 353Hz, 512Hz, 548Hz and 860Hz. The angle of incidence of the plane wave is marked.

To further investigate the effect of the cylinder on the acoustic field, the scattered acoustic field $p_s$ can be defined as the difference between the incident acoustic field $p_{inc}$, and the total acoustic field $p_t$:

$$p_s = p_t - p_{inc}. \tag{1}$$

The scattered acoustic pressure field has been calculated and plotted in a similar way to Figure 6, as shown in Figure 7. Whilst the total acoustic pressure plots in Figure 6 show the strongest effect on the total field at the 548Hz mode, the scattered acoustic pressure plots in Figure 7 clearly shows acoustic scattering at all four frequencies, with the reflected wave propagating away from the cylinder (in the positive $x$ direction) and an area of high scattering immediately behind the cylinder, where its presence creates a shadowing effect.

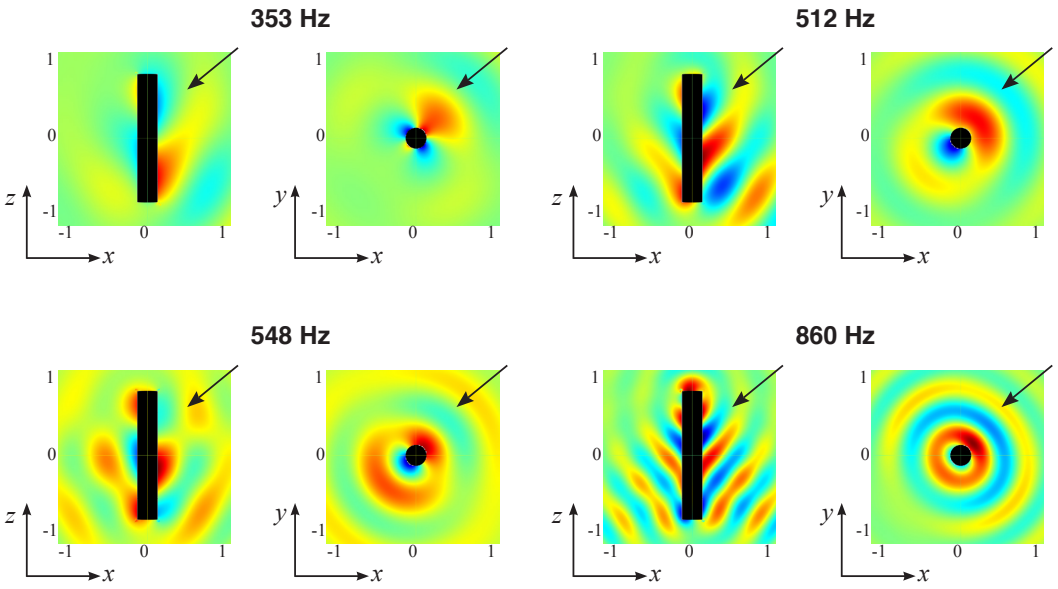


Figure 7: Predicted acoustic scattering when the cylinder is excited by an incident plane wave at 353Hz, 512Hz, 548Hz and 860Hz. The angle of incidence of the plane wave is marked.

To accurately assess how the acoustic scattering is affected by resonances within the cylinder, and to further benchmark the performance once active vibration control is implemented, the acoustic scattered power $W_{scat}$ is calculated as an integral of the scattered sound pressure over a far-field sphere enclosing the cylinder:

$$W_{scat} = \int_S \frac{|p_s^2|}{2\rho_0 c_0}. \tag{2}$$

As in Figure 5, this was computed and plotted over a range of frequencies. A similar process was carried out on a rigid cylinder model to provide a comparison. The resulting scattered power for the rigid and flexible cylinder models is shown in Figure 8, along with zoomed in plots that focus on the two main resonances of interest. It can be seen from Figure 8 that the acoustic scattering behaviour of both the rigid and flexible cylindrical shells are almost identical except for when the cylinder is excited at the 548Hz or 860Hz modes, at which points there are clear resonances in the scattered acoustic field, as shown in the two lower subplots.

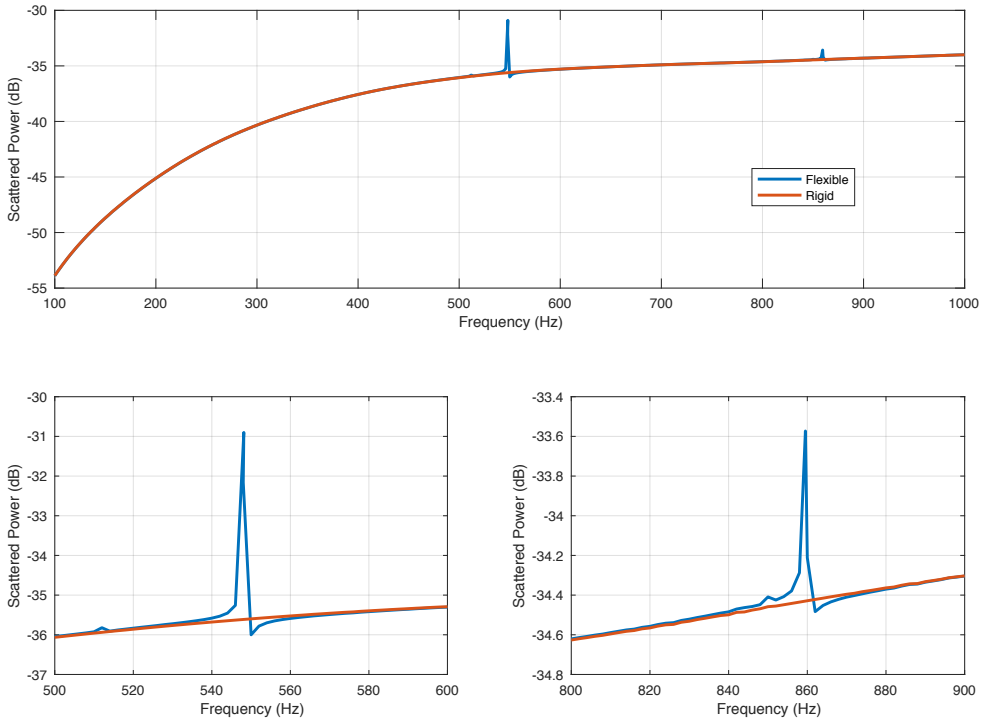


Figure 8: Total acoustic scattered power as a function of frequency, when excited by a plane wave from $\theta = 45$ $\phi = 45$. The bottom plots are zoomed in on two different frequency ranges to display the resonances of interest.

The results presented in Figure 8 are consistent with the analytical results shown by Bobrovnitskii [10], where the rigid cylinder behaves similarly to the flexible cylinder except at specific resonance peaks. Although the peak in the graph presented in [10] is at approximately $ka = 0.4$ whereas the peak presented in Figure 8 is at $ka \approx 1.1$, it should be noted that Bobrovnitskii's model was based on an external fluid of water rather than air. The effect of fluid loading on the cylinder will decrease the frequency of the structural resonances, therefore these results are still consistent.

# 3 Active Vibration Control

Figure 8 shows the scattered sound power spectra from the numerical model discussed above, for both a rigid and flexible scatterer. It has been discussed previously how the key difference is the presence of peaks in the scattered field of the flexible scatterer, caused by structural resonances within the cylindrical shell. This is further supported by the presentation of rigid scattering results by Williams [11] and Scandrett [13], both of which show consistently smooth scattering plots without the presence of sharp peaks. For many applications, it is likely to be these sharp peaks that cause the most coloration to the measured sound, rather than the smooth scattering curve caused by a rigid scatterer. Active vibration control can be used with accelerometers providing the error signal and structural actuators acting as control sources, in order to minimise the structural vibration of the cylinder. An Active Vibration Control system has thus been simulated within the framework of the numerical model, using accelerometers and control actuators attached to the surface of the cylinder.

## 3.1 Force-Sensor Configuration

An array of 97 velocity sensors and an array of 23 control forces have been defined over the surface of the cylinder, as shown in Figure 9. The response from each control force to every velocity sensor was firstly

calculated, leading to the construction of the plant matrix of complex transfer impedances $\mathbf{G}$.

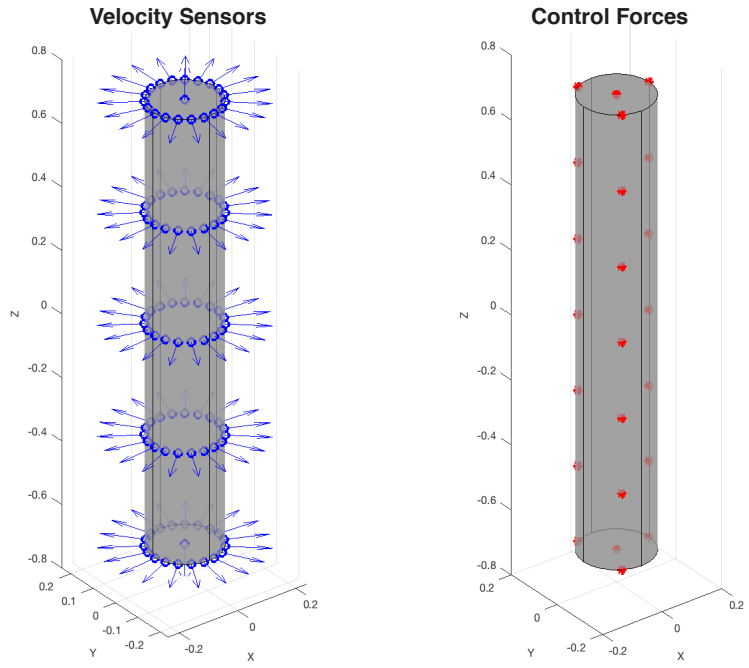


Figure 9: Location of the control forces and error sensors on the surface of the cylinder. Each control force acts inwards in the normal direction, whilst arrows mark the normal direction of each velocity sensor.

## 3.2 Active Vibration Control Formulation

The vector of velocities at the structural error sensors, $\mathbf{e}$, can be expressed as the linear superposition of the velocities due to the incident acoustic field, $\mathbf{d}$, and those due to the control actuators, which can be expressed as $\mathbf{Gf}$ where $\mathbf{f}$ is the vector of control forces. This gives the vector of error signals as

$$\mathbf{e} = \mathbf{d} + \mathbf{Gf}. \tag{3}$$

The vector of forces that minimises the sum of the squared error signals is then given by [14]

$$\mathbf{f_{opt}} = -\left(\mathbf{G}^H\mathbf{G} + \beta\mathbf{I}\right)^{-1}\mathbf{G}^H\mathbf{d}. \tag{4}$$

The suitable selection of the regularisation parameter $\beta$ facilitates a trade-off between performance and robustness; this will be considered below.

## 3.3 AVC Tuning & Performance

Using the equations and source/sensor positions discussed above, single tone active vibration control has been simulated for a range of frequencies between 100Hz and 1kHz. The effect of regularisation will first be investigated and optimised, before the predicted structural performance of the AVC system is presented. Finally, the effect that this has on the scattered field will be discussed.

### 3.3.1 Selection of the Regularisation Parameter

To investigate the effect of regularisation, the AVC model has been solved with increasing values of regularisation from $\beta = 1 \times 10^{-10}$ to $\beta = 1 \times 10^{10}$. In each case, the condition number of the matrix inversion $\left(\mathbf{G}^H\mathbf{G} + \beta\mathbf{I}\right)^{-1}$ has been calculated, which relates to the robustness of the system, and the achieved attenuation in structural velocity of the cylindrical shell has also been calculated. These are shown in Figure 10. As expected, it can be seen that high levels of regularisation result in a well conditioned inversion, however achieve limited attenuation. A value of $\beta = 1 \times 10^{-2}$ has been marked with a vertical red line, and provides a low condition number whilst maintaining reasonable attenuation performance of the AVC system, thus reaching a reasonable tradeoff between performance and robustness.

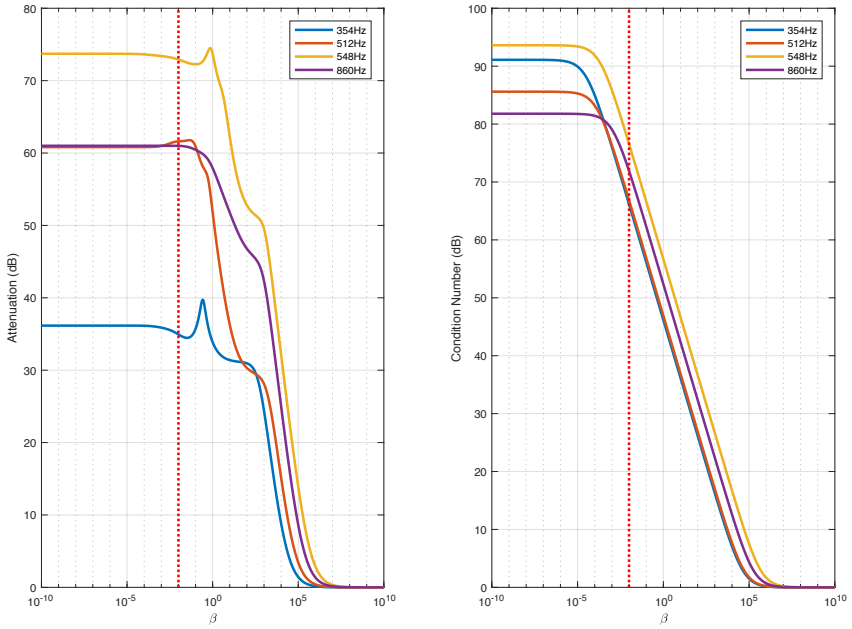


Figure 10: Condition number of matrix inverse, and achieved attenuation in structural acceleration, with varying amounts of regularisation at 354Hz, 512Hz, 548Hz and 860Hz. $\beta = 1 \times 10^{-2}$ is marked with a vertical red line.

### 3.3.2 Active Vibration Control Performance

Using Equations 3 and 4, as well as the matrix $\mathbf{G}$, the vector $\mathbf{d}$ and a value of $\beta = 1 \times 10^{-2}$, optimal control forces were calculated at each frequency. The resulting structural response before and after control is then shown in Figure 11. From these results it can be seen that a significant reduction in the structural velocity across the entire frequency range has been achieved. The structural velocity is reduced at every frequency, with the active vibration control effectively eliminating the resonance peaks completely. Although the structure is still vibrating, the magnitude of vibration is reduced sufficiently that it can be compared to a rigid body - that is, the velocity is close to zero.

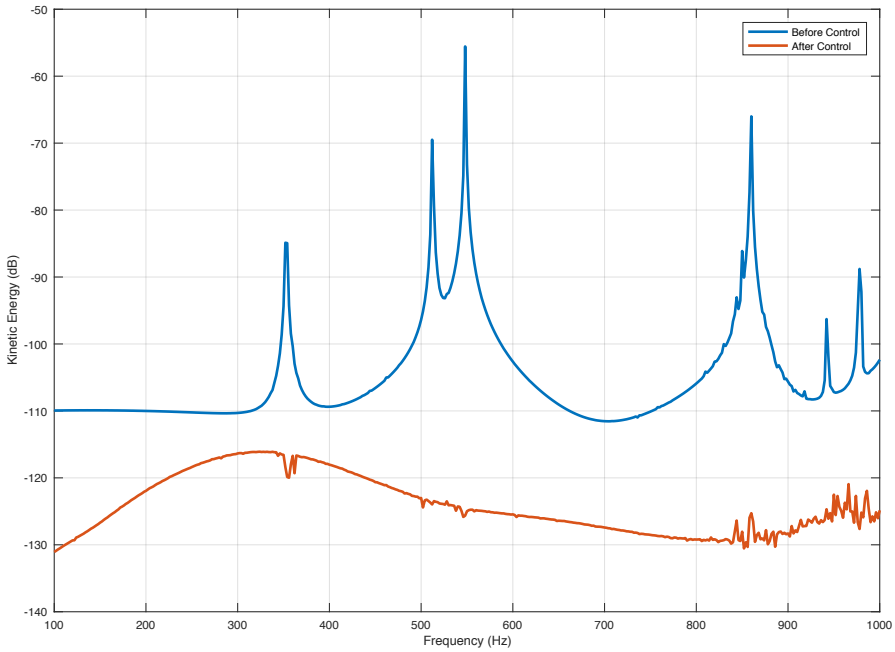


Figure 11: Kinetic energy before and after active vibration control

Using Equation 2, the acoustic scattered power has been computed before and after active vibration control, and these results are presented in Figure 12, along with the scattered sound power due to a rigid cylinder. From these results it can be seen that the scattered sound power for the flexible body before control shows significant peaks in the response, however these are attenuated by the AVC system and after control are consistent with a rigid cylinder.

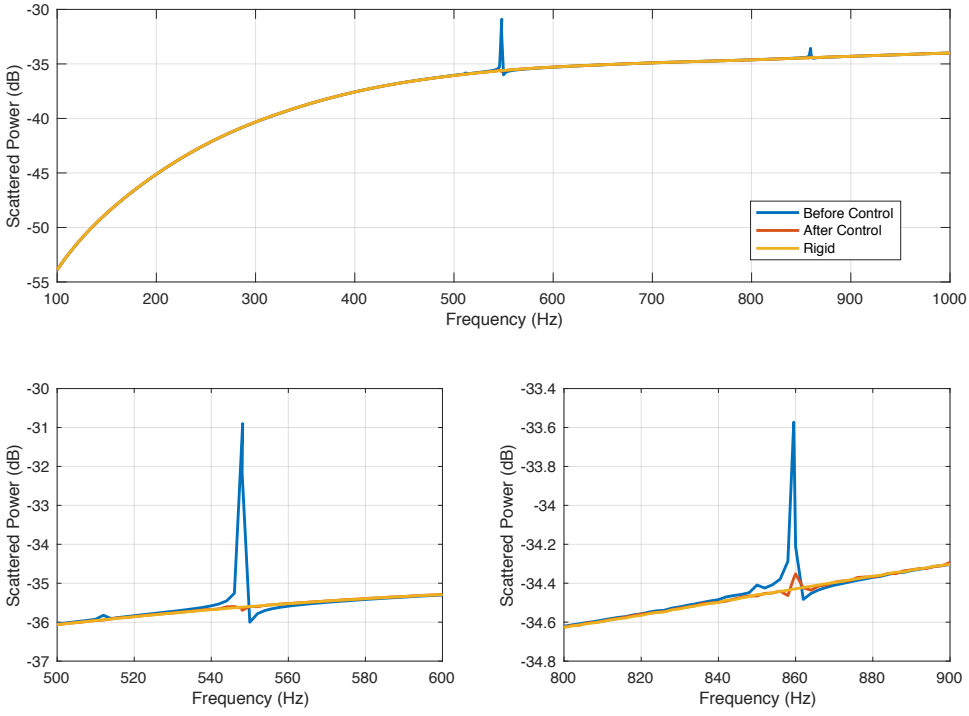


Figure 12: Acoustic scattered power before and after active vibration control, and for a rigid scatterer. The bottom plots are zoomed in on two different frequency ranges to display the resonances of interest.

# 4 Conclusions

This paper has investigated the effect of AVC on the acoustic scattering from a cylindrical scattering body. A numerical model of a flexible hollow cylindrical shell has been implemented and an eigenfrequency analysis has been carried out to identify the resonance frequencies of the cylinder, and to plot the corresponding mode shapes. Subsequently, the modelled cylinder was excited by an acoustic plane wave, and the resulting structural and acoustic responses were investigated.

Active vibration control was implemented on the cylindrical surface, reducing the structural velocity of the cylinder over a wide frequency band, but having significant effect when the cylinder is excited at resonance. The effect of this on the acoustic scattered field was investigated, and it was found that by implementing AVC the behaviour of the flexible cylinder converged to that of a rigid cylinder. The total acoustic scattered power was reduced by over 5dB when the cylinder was excited at its first bending mode. The amount of regularisation used in the calculation of optimal filters was investigated.

Although the structure has not been acoustically cloaked as it is still causing acoustic scattering, it no longer has resonances in the scattered field and therefore the detectability of the scattered field has been significantly reduced. For many applications (measurement microphones attached to a solid body, for example), full acoustic cloaking may not be necessary, and this reduction in sharp peaks in the scattered field may be sufficient.

# 5 Acknowledgements

The authors acknowledge the use of the IRIDIS High Performance Computing Facility, and associated support services at the University of Southampton, in the completion of this work. The first author is supported by an EPSRC iCASE studentship.

# References

[1] D. Eggler, H. Chung, F. Montiel, J. Pan, and N. Kessissoglou, "Active cloaking of rigid and elastic cylindrical scatterers," *Acoustics 2017*, no. 1, pp. 2–7, 2017.

[2] J. Cheer, "Active control of scattered acoustic fields: Cancellation, reproduction and cloaking," *The Journal of the Acoustical Society of America*, vol. 140, no. 3, pp. 1502–1512, 2016. [Online]. Available: http://dx.doi.org/10.1121/1.4962284

[3] E. Friot and C. Bordier, "Real-time active suppression of scattered acoustic radiation," *Journal of Sound and Vibration*, vol. 278, no. 3, pp. 563–580, 2004.

[4] E. Friot, R. Guillermin, and M. Winninger, "Active control of scattered acoustic radiation: A real-time implementation for a three-dimensional object," *Acta Acustica united with Acustica*, vol. 92, no. 2, pp. 278–288, 2006.

[5] N. Han, X. Qiu, and S. Feng, "Active control of three-dimension impulsive scattered radiation based on a prediction method," *Mechanical Systems and Signal Processing*, vol. 30, pp. 267–273, 2012. [Online]. Available: http://dx.doi.org/10.1016/j.ymssp.2012.01.023

[6] G. Caruso, S. Galeani, and L. Menini, "Active vibration control of an elastic plate using multiple piezoelectric sensors and actuators," *Simulation Modelling Practice and Theory*, vol. 11, no. 5-6, pp. 403–419, 2003.

[7] S. Daley, F. A. Johnson, J. B. Pearson, and R. Dixon, "Active vibration control for marine applications," *Control Engineering Practice*, vol. 12, no. 4, pp. 465–474, 2004.

[8] I. Bruant, L. Gallimard, and S. Nikoukar, "Optimal piezoelectric actuator and sensor location for active vibration control, using genetic algorithm," *Journal of Sound and Vibration*, vol. 329, no. 10, pp. 1615–1635, 2010. [Online]. Available: http://dx.doi.org/10.1016/j.jsv.2009.12.001

[9] C. R. Fuller, S. J. Elliott, and P. A. Nelson, "Active Control of Vibration," in *Academic Press*. Academic Press, 1997.

[10] Y. I. Bobrovnitskii, "A new impedance-based approach to analysis and control of sound scattering," *Journal of Sound and Vibration*, vol. 297, no. 3-5, pp. 743–760, 2006.

[11] E. G. Williams, *Fourier Acoustics - Sound Radiation and Nearfield Acoustical Holography*. Elsevier, 1999.

[12] A. Rona, "The acoustic resonance of rectangular and cylindrical cavities," *Proceedings of the 13th CEAS/AIAA Aeroacoustics Conference*, vol. 1, no. 3, pp. 1–12, 2007. [Online]. Available: http://hdl.handle.net/2381/1986

[13] C. Scandrett, "Scattering and active acoustic control from a submerged spherical shell," *The Journal of the Acoustical Society of America*, vol. 111, no. 2, p. 893, 2002. [Online]. Available: http://link.aip.org/link/JASMAN/v111/i2/p893/s1{&}Agg=doi

[14] S. J. Elliott, *Signal Processing for Active Control*. Academic Press, 2001.